Shape-Adaptive Kernel Density Estimation

L.E.N. Baakman

September 11, 2017

Abstract

Kernel density estimation has gained popularity in the past few years. Generally the methods use symmetric kernels, even though the data of which the density is estimated are not necessarily spread equally in all dimensions. To account for this asymmetric distribution of data we propose the use of shape adaptive kernels: kernels whose shape changes to fit the spread of the data in the local neighborhood of the point whose density is estimated. We compare the performance of the shape adaptive kernels on simulated datasets with known density fields. No significant differences in performance between the symmetric and the shape-adaptive estimator were found. Although the former outperformed the latter on points near the boundary of the datasets. In conclusion shape-adaptive kernels are a promising idea that warrants further research.

1 Introduction

Estimating densities with kernels has been fairly popular of late; in the medical field it has been used to predict dose-volume histograms, which are instrumental in the determination of radiation doses [7]. Ecologists have applied it to explore the habitats of seabirds [6]. Ferdosi et al. [4] have described it as "a critical first step in making progress in many areas of astronomy." Within this discipline density estimation is, among other things, used to estimate the density of the cosmic density field, which is required for the reconstruction of the large-scale structure of the universe.

Formally the aim of density estimation is to find the probability density $f(\mathbf{x})$ in the d-dimensional Euclidean space underlying N points $\mathbf{x}_1, \ldots, \mathbf{x}_N$, that have been selected independently from $f(\mathbf{x})$.

Kernel density estimation methods approximate $f(\mathbf{x})$ by placing bumps, referred to as kernels, on the different observations and summing these bumps to arrive at a final density estimate. This paper is concerned with a method to make the shape of the kernels adaptive to their local neighborhood. Before introducing the process used to determine the form of the kernel we first review the different symmetric kernel density estimation methods.

The Parzen approach [8] is one of the simplest kernel density estimation methods. It approximates the density of some pattern $\mathbf{x}$ according to:

$$\hat{f}(\mathbf{x}) = \frac{1}{N}\sum_{i=1}^{N} h^{-d} K\left(\frac{\mathbf{x}-\mathbf{x}_i}{h}\right). \qquad (1)$$

The shape of the used bumps is determined by the kernel function $K(\bullet)$, their width by the bandwidth h. The Parzen approach requires the kernel to be a probability density function, i.e. $K(\mathbf{x}) \geq 0$ and $\int K(\mathbf{x}) = 1$ [9]. The bandwidth directly influences the result of the density estimation process; a too small bandwidth results in a density estimate with spurious fine structures, whereas kernels that are too wide can oversmooth the density estimate. Kernel estimators, such as the Parzen approach, that use kernels of the same width for all $\mathbf{x}_i$, are called fixed-width estimators.

One downside of fixed-width methods is that the peakedness of the kernel is not data-responsive. Consequently in low density regions the density estimate will have peaks at the few sample points and be too low elsewhere. Whereas in areas with high density the Parzen estimate is spread out, as the sample points are more densely packed together[2]. Adaptive-width methods address this disadvantage of the fixed-width methods by allowing the width of the kernel to vary per data point. For example the estimator introduced by Breiman, Meisel, and Purcell uses the distance between $\mathbf{x}_i$ and the k-nearest neighbor of $\mathbf{x}_i$, denoted by $D_{i,k}$, to determine the width of the kernel:

$$\hat{f}(\mathbf{x}) = \frac{1}{N}\sum_{i=1}^{N} (\alpha \cdot D_{i,k})^{-d} K_{\mathcal{G}}\left(\frac{\mathbf{x}-\mathbf{x}_i}{\alpha \cdot D_{i,k}}\right). \qquad (2)$$

In this equation $K_{\mathcal{G}}$ is used to represent a Gaussian kernel, and α is a multiplicative constant. The values of both α and k can be determined with a minimization algorithm on a goodness of fit statistic. Comparing Equation (1) with (2) one finds that

the bandwidth h of the Parzen estimator is defined as $\alpha \cdot D_{i,k}$ in Equation (2). The factor $D_{i,k}$ depends on the local neighborhood of $\mathbf{x}_i$, in low density regions this factor is large, and the kernel spreads out due to its high bandwidth. In areas with relatively many data points the converse occurs.

Silverman [9] shows that the minimization procedure used by Breiman, Meisel, and Purcell implicitly uses a k-NN pilot estimate. If pilot estimates, denoted by $\tilde{f}(\bullet)$, are used explicitly, the density estimation process becomes:

(i) Compute pilot densities with some estimator that ensures that $\forall i\ \tilde{f}(\mathbf{x}_i) > 0$.

(ii) Define local bandwidths γ_i as

$$\gamma_i = \left(\frac{\tilde{f}(\mathbf{x}_i)}{\mathrm{GM}\left(\tilde{f}(\mathbf{x}_0), \ldots, \tilde{f}(\mathbf{x}_N)\right)} \right)^{-\beta}, \quad (3)$$

where GM denotes the geometric mean and the sensitivity parameter β must lie in the range $[0,1]$.

(iii) Compute the adaptive kernel estimate as

$$\hat{f}(\mathbf{x}) = \frac{1}{N} \sum_{i=1}^{N} (h \cdot \gamma_i)^{-d} K\left(\frac{\mathbf{x} - \mathbf{x}_i}{h \cdot \gamma_i} \right) \quad (4)$$

with K integrating to unity.

Since the pilot densities computed in step (i) do not need to be sensitive to the fine details of the pilot estimate a convenient method, e.g. the Parzen approach, can be used to estimate them [9]. The local bandwidths, computed in step (ii), depend on the exponent β. The higher this value is the more sensitive the local bandwidths are to variations in the pilot densities. Choosing $\beta = 0$ reduces Equation (4) to a fixed-width method. In the literature two values of β are prevalent. Breiman, Meisel, and Purcell [2] argue that choosing $\beta = {}^1/_d$ ensures that the number of observations covered by the kernel will be approximately the same in all areas of the data. Whereas Silverman [9] favors $\beta = {}^1/_2$ independent of the dimension of the data, as this value results in a bias that can be shown to be of a smaller order than that of the fixed-width kernel estimate.

One disadvantage of the Breiman estimator is its computational complexity. This is partially due to the use of a Gaussian kernel. Because of the infinite base of this kernel an exponential function has to be evaluated N times to estimate the density of one data point. Wilkinson and Meijer [10] address this in their Modified Breiman Estimator (MBE) by replacing the Gaussian kernel with a spherical Epanechnikov kernel in both the computation of the pilot densities and in the final density estimate. This kernel is defined as

$$K_{\mathcal{E}}(\mathbf{x}) = \begin{cases} \frac{d+2}{2c_d}(1 - \mathbf{x} \cdot \mathbf{x}) & \text{if } \mathbf{x} \cdot \mathbf{x} < 1 \\ 0 & \text{otherwise} \end{cases} \quad (5)$$

where c_d denotes the volume of the d-dimensional unit sphere [3]. It should be noted that the kernel defined in Equation (5) does not have unit variance. This can be corrected by multiplying the bandwidth, h, with the square root of the variance of $K_{\mathcal{E}}$, i.e. $\sqrt{5}$. There are two advantages to using this kernel, firstly it is computationally much simpler than the Gaussian kernel, in part due to its finite base, and secondly it is optimal in the sense of the Mean Integrated Square Error (MISE) [3]. One downside of this kernel is that it is not continuously differentiable. This is irrelevant when computing the pilot densities, however for the final densities it is a trade off between a continuously differentiable density estimate and a density estimator that has a low computational complexity. Wilkinson and Meijer [10] compute the global bandwidth according to

$$h = \sigma \cdot N^{-1/(d+4)} \left(\frac{8(d+4) \cdot \left(2\sqrt{\pi}\right)^d}{c_d} \right)^{\frac{1}{d+4}}, \quad (6)$$

where σ represents the square root of the average of the variances of the different dimensions. The final densities are estimated with Equation (4), using the general and local bandwidths estimated with Equation (6) and (3), respectively.

Ferdosi et al. [4] consider the application of density estimation on large datasets, i.e. sets with more than 50 000 points with the dimension of the data points ranging from ten to hundreds of elements. They use the MBE, but introduce a computationally less complex method to estimate the bandwidth. First an intermediate bandwidth for each dimension l of the data is computed with

$$h_l = \frac{P_{80}(l) - P_{20}(l)}{\log N}, l = 1, \ldots, d, \quad (7)$$

where $P_{20}(l)$ and $P_{80}(l)$ are the twentieth and eightieth percentile of the data in dimension l, respectively. From these intermediate bandwidths the minimum is used as h.

Although the widths of the kernels of the discussed adaptive-width methods are sensitive to the data, the shapes of the kernels depend only on its definition. To further increase the responsiveness of the estimator to the data we propose the use of shape-adaptive kernels; not only the width but also

the shape of these kernels is steered by the local neighborhood of the data.

A possible disadvantage of these shape-adaptive kernels is that in regions where the density of sample points is low, the number of data points is insufficient to reliably compute the shape of the kernel. Therefore we let the amount of influence exerted by the local data on the shape of the kernel depend on the number of data points in the local neighborhood.

This paper is organized as follows. Section 2 introduces the proposed shape-adaptive kernels. The experiment used to investigate the performance of these kernels is discussed in Section 3, the results are presented in Section 4. They are discussed in Section 5, and the reached conclusion can be found in Section 6.

2 Method

We use shape adaptive kernels in combination with the Modified Breiman Estimator introduced by Wilkinson and Meijer [10], the resulting estimator is henceforth also referred to as the shape-adaptive Modified Breiman Estimator (saMBE). For its lower computational complexity we use the method introduced by Ferdosi et al. [4], defined in Equation (7), to compute the general bandwidth. Pilot densities are computed according to Equation (1), with an Epanechnikov kernel. Since using $\beta = {}^1/_2$ in Equation (3) results in a final density approximation with a lower mean squared error than using $\beta = {}^1/_d$. We use the first when computing the local bandwidths. The final density estimate is computed according to:

$$\hat{f}(\mathbf{x}) = \frac{1}{N}\sum_{i=1}^{N} \frac{1}{\det(\mathbf{H}_i)} K_{\mathcal{E}}\left(\mathbf{H}_i^{-1}(\mathbf{x}-\mathbf{x}_i)\right). \qquad (8)$$

The shape of the kernel $K_{\mathcal{E}}(\bullet)$ is determined by the bandwidth matrix $\mathbf{H}_i$ [5]. If $\mathbf{H}_i = h \cdot \gamma_i \cdot \mathbb{I}_{d\times d}$, Equation (8) reduces to Equation (4).

For each data point $\mathbf{x}_i$ that is used in the density estimation of some pattern $\mathbf{x}_j$, the bandwidth matrix is determined according to these steps:

(i) Find $C_{\mathbf{x}_i}$, the k-nearest neighbors of $\mathbf{x}_i$.

(ii) Compute Σ, the unbiased covariance matrix of the local neighborhood $C_{\mathbf{x}_i}$.

(iii) Determine $\mathbf{H}_i$ by scaling Σ with

$$s = h \cdot \gamma_i \left(\prod_{l=1}^{d} \lambda_l\right)^{-\frac{1}{d}} \qquad (9)$$

where $\lambda_1, \cdots, \lambda_d$ are the eigenvalues of Σ.

Step (i) determines the local neighborhood of $\mathbf{x}_i$ with a k-nearest neighbors search in a KD-tree [1], with Euclidean distance as the distance metric. We follow Silverman's [9] recommendation of choosing $k = \sqrt{N}$. To ensure that Σ is nonsingular we also need $k > d$, therefore

$$k = \max\left(\left\lfloor\sqrt{N}\right\rceil, d\right) + 1.$$

Using a KD-tree for the k-nearest neighbors search instead of the naive implementation, significantly improves the time complexity of finding $\mathbf{H}_i$. The downside of using a space partitioning tree is that $C_{\mathbf{x}_i}$ is an approximation of the actual neighborhood, as long as k is rather large the use of an approximation instead of the exact k-nearest neighbors should not impact the final kernel result strongly. We use k-NN rather than a fixed-radius neighborhood to ensure that, independent of the sparsity of the data, the kernel shape is always based on a reasonable number of data points.

The basis shape of the kernel is determined in step (ii). The covariance matrix ensures that the major axis of the kernel has the same direction as the maximum variance of the data.

The scaling factor computed in step (iii) ensures that the kernels used in the density estimation of different patterns have a comparable domain. Equation (9) scales the bandwidth matrix in such a way that the volume of the ellipsoid defined by the eigenvectors and values of $\mathbf{H}_i$ is equal to that of the eigenellipsoid of the bandwidth matrix that is implicitly used in Equation (4).

3 Experiment

We contrast the performance of the shape-adaptive and the symmetric Modified Breiman Estimator on simulated datasets with known density fields. This allows us to test how well the proposed method can recover simple density distributions in comparison to an existing method. We distinguish two types of datasets: datasets consisting of a single Gaussian distribution and noise, defined in Section 3.1 and datasets containing multiple Gaussian distributions embed in noise, these sets are presented in Section 3.2.

To quantify the performance of the estimators we use the mean squared error (MSE):

$$\mathrm{MSE}\left(\hat{f}(\bullet)\right) = \frac{1}{N}\sum_{j=1}^{N}\left(\hat{f}(\mathbf{x}_j) - f(\mathbf{x}_j)\right)^2.$$

3.1 Datasets with a Single Gaussian

Figure 1 shows a scatter plot representation of the datasets containing a single Gaussian distribution defined in Table 1.

The Gaussian components of these datasets progress from a sphere, i.e. dataset S_1, to an increasingly more elongated ellipsoid. This makes it possible to investigate the influence of how strongly elongated the distribution is on the density estimate. The first dataset is a simple spherical Gaussian distribution centered in a uniform random background. The covariance matrix of the Gaussian component in S_2 is created from S_1 by squaring one of the eigenvalues of the covariance matrix, and taking the square root of the other two eigenvalues, without changing the eigenvectors. The resulting covariance matrix defines an eigenellipse with the same volume as the one defined by S_1. The Gaussian component of dataset S_3 changes the shape of the eigenellipse of the Gaussian component by lengthening one of the minor axes, and shortening the other. The Gaussian component in S_4 is spread out more along the y-axis and less along the z-axis, than the Gaussian component in dataset S_3.

We expect the Modified Breiman Estimator and its shape-adaptive cousin to perform comparably on dataset S_1, since due to the symmetric shape of the Gaussian distribution no advantage should be gained by using a shape-adaptive kernel. As the Gaussian distribution is more and more elongated, the advantage of using saMBE should become more pronounced.

3.2 Datasets with Multiple Gaussians

Table 2 defines the datasets that consist of uniform random noise and multiple Gaussian distributions, a scatter plot representation of these sets is shown in Figure 2. Dataset M_1 consists of two Gaussian distributions, that are unlikely to overlap, embedded in noise, the first Gaussian component is significantly denser than the second. The procedure outlined in Section 3.1 for the creation of dataset S_2 was used to derive dataset M_2 from set M_1. Dataset M_3 embeds four non-overlapping Gaussians, with eigenspheres with notably differencing radii, in the uniform random background. The last dataset, M_4, is a variation on M_3, created with method that was used for the definition of dataset S_2 from S_1.

We expect to find hardly any difference in performance between the classifiers on dataset M_1 and M_3. Given the shape of the Gaussian distributions embedded in dataset M_2 and M_4 we hypothesize that saMBE outperforms MBE on these sets.

Ferdosi et al. [4] found that the Modified Breiman Estimator resulted in lower integrated squared errors if fewer Gaussian distributions were present in the datasets. Since the presented datasets are comparable to those used by Ferdosi et al. we expect to find the same influence of the number of distributions on the error.

4 Results

This section presents the results of the experiments described in Section 3. We compare the performance of the two estimators on each dataset with the mean squared error and visually with plots. All plots associated with a single dataset have the same domain and range, to allow for easy comparison of the results within a dataset. The horizontal axis is used to represent the known densities, its range is such that each known density can be shown. The estimated densities are shown on the vertical axis, the length of these axes is such that they are long enough to represent every estimated density for that dataset, independent of the used estimator. The black line in each plot illustrates the line all points would lie on if a perfect estimator was used, i.e. the line $x = x$. The colors of the points in these plot correspond to the colors of the elements of the datasets in Tables 1 and 2.

Section 4.1 presents the results of the datasets that contain a single Gaussian, in Section 4.2 the results of the datasets that consist of noise and multiple Gaussian distributions are presented.

4.1 Datasets with a Single Gaussian

This section compares the performance of the Modified Breiman Estimator and a shape-adaptive variant on datasets that contain one Gaussian, i.e. dataset S_1, S_2, S_3, and S_4. Comparing the mean squared errors of the MBE with those of saMBE in Table 3 we find that the two estimators perform comparably, but that the fixed-shape estimator always gives a slightly lower mean squared error. This is confirmed by the visualization of the result in Figure 3 where hardly any difference is visible between Figures 3(a) to 3(d) and Figures 3(e) to 3(h), respectively.

Comparing Figure 3(a) with Figure 3(e) we find hardly any difference between the results of the two estimators, saMBE overshoots some densities more than MBE, but otherwise the results seem identical, which fits with the small difference in mean square error. Reviewing the mean squared errors

Before Final Version: Remove ticks and labels.

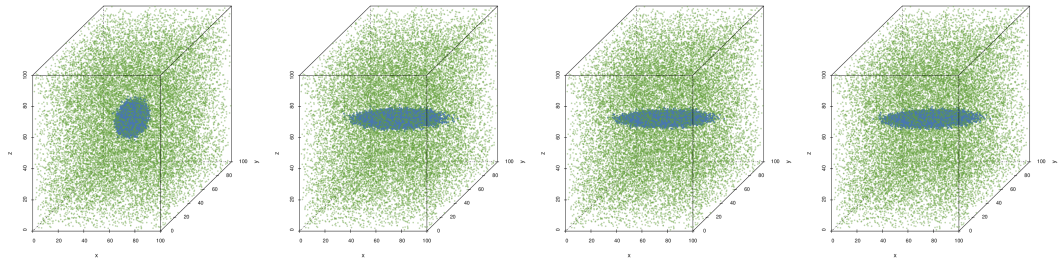

(a) *Set* S_1 **(b)** *Set* S_2 **(c)** *Set* S_3 **(d)** *Set* S_4

Figure 1: *Scatter plot representation of the datasets defined in Table 1. The used colors correspond to those associated with the different components in Table 1.*

Set		Component	Number	Distribution
S_1	■	Trivariate Gaussian	4.0×10^4	$\mathcal{N}([50,50,50],\text{diag}(11))$
	●	Uniform random background	2.0×10^4	$\mathcal{U}([0,0,0],[100,100,100])$
S_2	■	Trivariate Gaussian	4.0×10^4	$\mathcal{N}([50,50,50],\text{diag}([11,\sqrt{11},\sqrt{11}]))$
	●	Uniform random background	2.0×10^4	$\mathcal{U}([0,0,0],[100,100,100])$
S_3	■	Trivariate Gaussian	4.0×10^4	$\mathcal{N}([50,50,50],\text{diag}([11,2*\sqrt{11},{}^1\!/_2\sqrt{11}]))$
	●	Uniform random background	2.0×10^4	$\mathcal{U}([0,0,0],[100,100,100])$
S_4	■	Trivariate Gaussian	4.0×10^4	$\mathcal{N}([50,50,50],\text{diag}([11^2,11,1]))$
	●	Uniform random background	2.0×10^4	$\mathcal{U}([0,0,0],[100,100,100])$

Table 1: *The datasets containing a single Gaussian distribution embed in uniform noise. The column 'Number' indicates for each component the number of patterns sampled from it.* $\mathcal{N}(\mu,\Sigma)$ *denotes a Gaussian distribution with mean* μ *and covariance matrix* Σ*. A diagonal matrix with the values* $x_1,\cdots,x_d$ *on the diagonal is represented as* $\text{diag}([x_1,\cdots,x_d])$*, a scalar matrix with x on the diagonal is shown as* $\text{diag}(x)$*.* $\mathcal{U}(a,b)$ *denotes a uniform distribution with its minimum and maximum set to a and b, respectively. The second column presents the symbol used to represent this component in plots throughout the paper.*

Set		Component	Number	Distribution
M_1	■	Trivariate Gaussian 1	2.0×10^4	$\mathcal{N}([25,25,25],\text{diag}(5))$
	▲	Trivariate Gaussian 2	2.0×10^4	$\mathcal{N}([45,45,45],\text{diag}(11))$
	●	Uniform random background	2.0×10^4	$\mathcal{U}([0,0,0],[100,100,100])$
M_2	■	Trivariate Gaussian 1	2.0×10^4	$\mathcal{N}([25,25,25],\text{diag}([5^2,\sqrt{5},\sqrt{5}]))$
	▲	Trivariate Gaussian 2	2.0×10^4	$\mathcal{N}([45,45,45],\text{diag}([\sqrt{11},\sqrt{11},11^2]))$
	●	Uniform random background	2.0×10^4	$\mathcal{U}([0,0,0],[100,100,100])$
M_3	■	Trivariate Gaussian 1	2.0×10^4	$\mathcal{N}([24,10,10],\text{diag}(2))$
	▲	Trivariate Gaussian 2	2.0×10^4	$\mathcal{N}([33,70,40],\text{diag}(10))$
	♦	Trivariate Gaussian 3	2.0×10^4	$\mathcal{N}([90,20,80],\text{diag}(1))$
	✳	Trivariate Gaussian 4	2.0×10^4	$\mathcal{N}([60,80,23],\text{diag}(5))$
	●	Uniform random background	4.0×10^4	$\mathcal{U}([0,0,0],[100,100,100])$
M_4	■	Trivariate Gaussian 1	2.0×10^4	$\mathcal{N}([24,10,10],\text{diag}([4,\sqrt{2},\sqrt{2}]))$
	▲	Trivariate Gaussian 2	2.0×10^4	$\mathcal{N}([33,70,40],\text{diag}([\sqrt{10},\sqrt{10},100]))$
	♦	Trivariate Gaussian 3	2.0×10^4	$\mathcal{N}([90,20,80],\text{diag}(1))$
	✳	Trivariate Gaussian 4	2.0×10^4	$\mathcal{N}([60,80,23],\text{diag}([25,\sqrt{5},\sqrt{5}]))$
	●	Uniform random background	4.0×10^4	$\mathcal{U}([0,0,0],[100,100,100])$

Table 2: *The datasets with multiple Gaussian distributions embedded in uniform noise. This table has the same structure and uses the same notation as Table 1.*

Before Final Version: Remove ticks and labels.

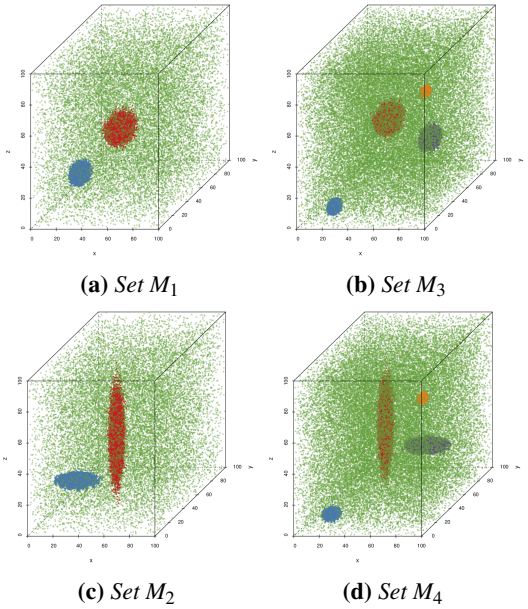

(a) *Set* M_1 **(b)** *Set* M_3 **(c)** *Set* M_2 **(d)** *Set* M_4

Figure 2: *Scatter plot representation of the datasets defined in Table 2, the colors used for the different components correspond to those in Table 2.*

	Estimator	
Set	MBE	saMBE
S_1	8.306×10^{-9}	8.909×10^{-9}
S_2	1.490×10^{-8}	1.540×10^{-8}
S_3	2.937×10^{-8}	2.963×10^{-8}
S_4	5.572×10^{-8}	5.585×10^{-8}

Table 3: *Performance of the Modified Breiman Estimator with fixed-shaped and shape-adaptive kernels on the datasets with a single Gaussian.*

of the components of this dataset we find that MBE slightly outperforms saMBE on both datasets.

Figures 3(b) and 3(f) confirm what the MSE already told us, there is hardly any difference in performance between the two estimators. There is no difference within the estimators between components.

Based on the differences between Figures 3(c) and 3(g) we can at best conclude that the shape-adaptive estimator overestimates the densities slightly more than the fixed-shape estimator. The differences between estimators within components are not significantly large.

Figures 3(d) and 3(h) supports the MSE in that there hardly any difference in estimated densities between the two estimators on dataset S_4. Furthermore within components the differences between the estimators are also negligible.

	Estimator	
Set	MBE	saMBE
M_1	5.058×10^{-8}	5.050×10^{-8}
M_2	5.147×10^{-8}	5.168×10^{-8}
M_3	4.375×10^{-6}	4.463×10^{-6}
M_4	4.189×10^{-6}	4.284×10^{-6}

Table 4: *Performance of the symmetric and the shape-adaptive Modified Breiman Estimator on the datasets containing multiple Gaussian distributions.*

We have found no direct correlation between the length of largest minor axis of the eigenellipse and the performance of the estimators, e.g. the MSE of S_3 is lower than that of S_2. Comparing the performance of both estimators on between dataset S_1 and S_4 suggest that lengthening the major axes has a negative influence on the performance of the estimator.

4.2 Datasets with Multiple Gaussians

In this section we present the results of the two estimators on dataset M_1, M_2, M_3, M_4.

Comparing Figure 4(a) with Figure 4(c) we find that both estimators underestimate the density and that the densities estimated by the saMBE are spread out more than those estimated by MBE. In spite of this the difference in mean squared error between the two estimators is small enough to be insignificant. The same holds for the mean squared error of the individual components.

Figures 4(b) and 4(d) show the same general trend as Figures 4(a) and 4(c): both estimators underestimate, the shape-adaptive estimator less so than the symmetric estimator, but the differences between the two estimators are small. The differences in MSE within the difference components between the estimators are negligible. Comparing the performance of the estimators between datasets M_1 and M_2 we find that the performance of both estimators hardly suffers from the elongation of the Gaussians.

Figures 5(a) and 5(c) clearly show that both estimators significantly underestimate the true density, saMBE more so than MBE. Comparing the mean squared error of the different components we find that both estimators performed worst on the densest component, and best on the component with the highest value on the diagonal of its covariance.

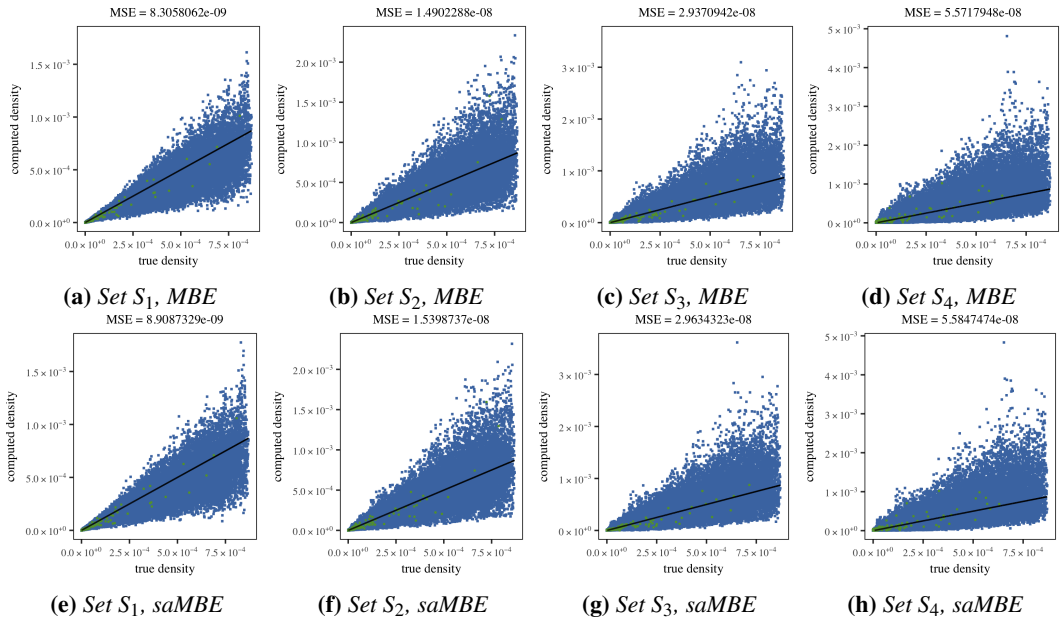

(a) *Set S_1, MBE* **(b)** *Set S_2, MBE* **(c)** *Set S_3, MBE* **(d)** *Set S_4, MBE*

(e) *Set S_1, saMBE* **(f)** *Set S_2, saMBE* **(g)** *Set S_3, saMBE* **(h)** *Set S_4, saMBE*

Figure 3: *Plot of the estimated density as a function of the known density of the datasets with a single Gaussian by (a)-(d) MBE and (e)-(h) saMBE.*

There is no significant difference between the estimators within the different components.

Figures 5(b) and 5(d) shows the same underestimating of densities as the plot of the plots associated with datasets M_3. Compared to densities estimated for that dataset the range of densities estimated by both estimators for dataset M_4 is greater. The difference in mean squared error within both the complete set and its components between the two estimators is negligible. Contrary to our expectations both estimators perform better on the elongated dataset, i.e. M_3, than on the spherical set.

In general we have found that the number of Gaussian distributions embed in the noise negatively influences the performance of both estimators. Furthermore the denser a Gaussian distribution is, the more difficulty the estimators have with correctly approximating the density of the points sampled from it.

By comparing the mean squared error of the different components of the datasets we have also found that both estimators are better at estimating the density of points sample from uniform random noise than points sampled from a Gaussian distribution.

5 Discussion

This section is concerned with the difference in performance between the two estimators within datasets. Section 5.1 focuses on datasets containing a single Gaussian, whereas Section 5.2 discusses the four other datasets.

5.1 Datasets with a Single Gaussian

The scatter plots of the datasets with a single Gaussian in Figure 6 emphasize the points where the absolute error of the symmetric estimator is smaller than that of the shape-adaptive estimator.

Figure 6(a) shows that the shape-adaptive estimator outperforms the symmetric estimator on most points near the boundary of the dataset. Based on this figure on might also conclude that in general MBE results in a lower error than saMBE on the other points, however the raw data shows that on 5.272×10^1 %% of the full dataset, and on 5.566×10^1 % % of the Gaussian component the symmetric estimator results in a lower absolute error. Reviewing the shape of the kernels used for the points in dataset S_1 we find that the used kernels are all near spherical. The kernels with the largest differences between their eigenvalues are associated with points near the boundary of the dataset. The largest differences in error between the two estimators can be found near the center of the Gaussian

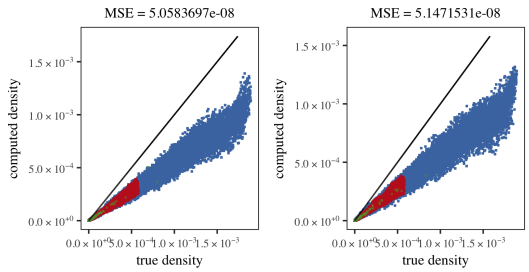

(a) *Set M_1, MBE* **(b)** *Set M_2, MBE*

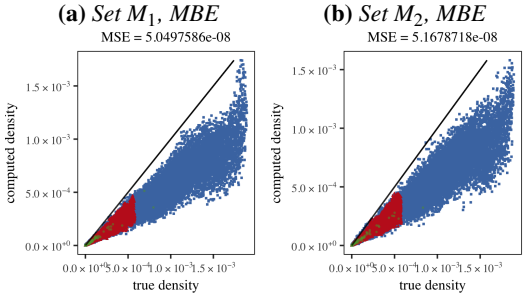

(c) *Set M_1, saMBE* **(d)** *Set M_2, saMBE*

Figure 4: *Plots of the true versus estimated density of datasets M_1 and M_2 for the shape-adaptive and the symmetric Modified Breiman Estimator.*

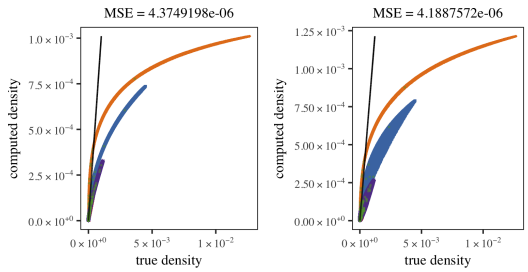

(a) *Set M_3, MBE* **(b)** *Set M_4, MBE*

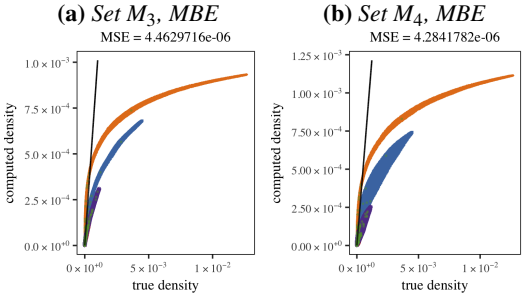

(c) *Set M_3, saMBE* **(d)** *Set M_4, saMBE*

Figure 5: *The estimated density plotted as a function of the true density for datasets M_3 and M_4 for MBE and saMBE.*

component, where the shape-adaptive kernels are relatively spherical. The difference between the two estimators at these points is caused by the number of points used to estimate the density, for most of these points saMBE uses too many points which results in an overestimated density.

The results in Figure 6(b) are comparable to those in Figure 1(a), however there seem to be fewer points of the noise component where the absolute error of using the symmetric-kernel is lower than using a shape-adaptive kernel. Reviewing the raw data shows that this difference is primarily caused by the 7.803×10^3 % points for which both estimators estimate the same density. Due to the elongated shape of the distribution its shape influences the kernel of fewer shapes of the noise component resulting in more spherical kernels, which results in the same density estimate for a larger number of points. As in dataset S_1 the points with the most ellipsoidal kernels are positioned near the boundaries of the dataset, where saMBE outperforms MBE. The points whose differences in estimated densities are largest are, as in dataset S_1, found near the mean of the Gaussian distribution. At first this seems counterintuitive since the kernels are relatively spherical near the Gaussian component, however we expect that due to the high density of points in that area a small change to the shape of the kernel has a large effect. This is confirmed by the large differences in the number of patterns that are used in the density estimate of the points near the mean of the Gaussian component between the two estimators.

In Figure 6(c) we observe that the MBE outperforms saMBE on very few points in dataset S_3, to be exact on 92.71 % percent of the points the absolute error of the shape-adaptive estimator was at least as low as the error of the symmetric estimator. Once again we attribute this difference in performance to the elongated shape of the Gaussian component. Reviewing the shape of the kernel we find kernels with a strongly adapted shape both near the boundary of the dataset, where saMBE outperforms MBE, and near the Gaussian component. Near the mean of this component we also find the biggest differences in estimated densities between the two estimators.

The effect of how elongated the Gaussian component is on how well the density of the noise is estimated is even strong in dataset S_4, as illustrated in Figure 6(d). The density estimate of the two estimates is the same for 9.540×10^1 %% of the points drawn from the uniform distribution, contrastingly this is only the case for 5.575 %% of the points from the Gaussian component. As in dataset S_3 the shape of the kernels is most strongly influenced by the data near the boundaries of the dataset and the Gaussian component. The largest differences between the result of the two estimators are, comparable to what we observed in dataset S_3, found near the mean of

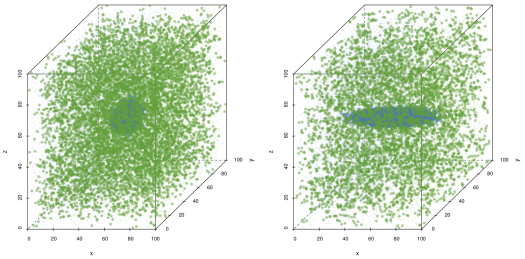

(a) *Dataset* S_1 **(b)** *Dataset* S_2

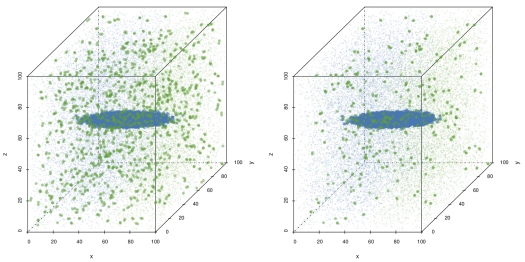

(c) *Dataset* S_3 **(d)** *Dataset* S_4

Figure 6: *Low opacity scatter plot of dataset (a)* S_1*, (b)* S_2*, (c)* S_3*, and(d)* S_4*, with an overlay of larger points with a higher opacity where the absolute error of saMBE is larger than or equal to the absolute error of MBE.*

the Gaussian component.

In general we have found that if the Gaussian component is strongly elongated, as in dataset S_3 and S_4, the shape of the kernels near the mean of the Gaussian component is influenced, whereas the spherical and ellipsoidal Gaussian component in dataset S_1 and S_2, respectively, hardly influences the shape of the kernels of the data points near its mean. We expect that this is caused by a lower physical density of points near the means of the more spherical Gaussians. In spite of this difference between the four datasets, in all datasets the difference in estimated density between the estimators is largest near the mean of the Gaussian component. We expect that this is due to the relative high density of points at this location, which causes small differences in the shapes of the kernels to have a large effect on the final density.

5.2 Datasets with Multiple Gaussians

In Section 4.2 we observed that the differences in performance between the two estimators are small.

Plotting the MBE density as a function of the saMBE density for dataset M_1 and M_2, see Figure 7, we find that saMBE generally estimates densities to be higher, and nearer to the true density, than MBE.

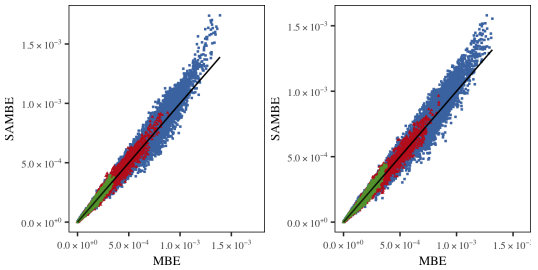

(a) *Dataset* M_1 **(b)** *Dataset* M_2

Figure 7: *Plots of the density estimated by saMBE as a function of those estimated by MBE for dataset (a)* M_1 *and (b)* M_2*.*

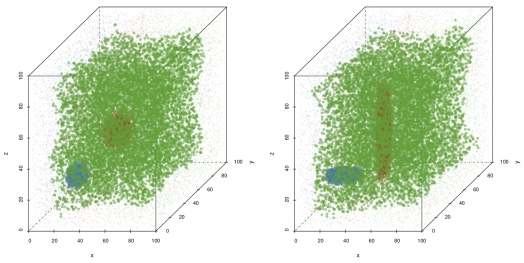

(a) *Dataset* M_1 **(b)** *Dataset* M_2

Figure 8: *Low opacity scatter plot of dataset (a)* M_1 *and (b)* M_2 *with an overlay of high opacity larger points where the absolute error of MBE is smaller than the absolute error of saMBE.*

To investigate the cause of this effect we created **??** in which the point on which the absolute error of the MBE was lower than the absolute error of the saMBE are emphasized. This plot shows that the shape-adaptive estimator outperforms the symmetric estimator on the boundary of both datasets, however the symmetric estimators seem to perform better on the center of the dataset where most points are located. It should be noted that counting the points in the center of the datasets were one estimators outperforms the other shows that the density of only approximately half of the are better estimated by the symmetric kernel. Neither dataset shows a correlation between the distance to the mean, the error and the used estimator.

Plotting the densities estimated by saMBE versus the densities estimated by MBE in Figure 9 shows that the differences between the estimators are as small as indicated by the mean squared error for nearly all points, saMBE slightly underestimates points drawn from the noise that has a high density. As the noise component by itself has an uniform density these points noise points are quite likely positioned near the center of one of the Gaus-

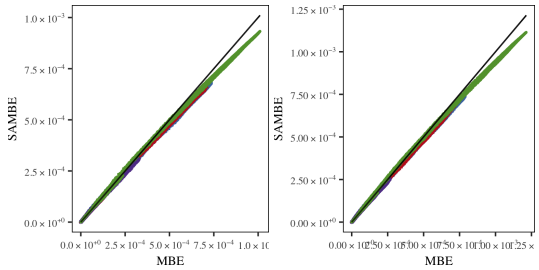

(a) *Dataset* M_3 **(b)** *Dataset* M_4

Figure 9: *Plots of the density estimated by saMBE as a function of those estimated by MBE for dataset (a)* M_1 *and (b)* M_2*.*

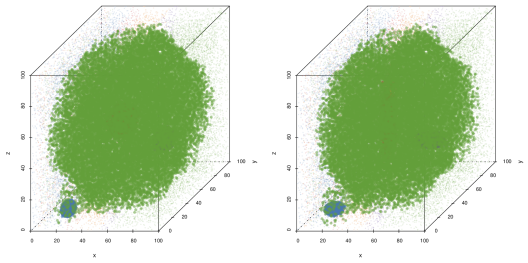

(a) *Dataset* M_3 **(b)** *Dataset* M_4

Figure 10: *Low opacity scatter plot of dataset (a)* M_1 *and (b)* M_2 *with the points where the absolute error of MBE is smaller than the absolute error of saMBE emphasized.*

sian components. Figure 10 shows that the shape-adaptive estimator outperforms the symmetric estimator consistently on points near the boundary of the dataset. Although it is not visible due to occlusion in Figures 10(a) and 10(b) approximately half of the points in the center have a lower absolute error for saMBE than for MBE. Taking a closer look at the Gaussians we find a correlation between which estimator has the lowest absolute error on a point and the distance of that point to the mean. For dataset M_3 we can say that saMBE performs better on points farther away from the mean, whereas MBE is better in approximating the density of points nearer to the mean of a distribution. In M_4 this effect is even stronger.

Interestingly the shape defined by the points where the absolute error of MBE is lower than that of saMBE defines a square in the dataset with two Gaussian components and approximately a sphere in the dataset with four Gaussian components. We expect that this difference is caused by the Gaussian components that are nearer to the boundaries in dataset M_3 and M_4.

In all datasets we have found a large difference in the shape of the kernels near the boundaries of the dataset. Kernels of a point near an edge of the dataset cube have their shortest minor axis perpendicular to the direction of the edge, to account for the lack of data points in that direction. This boundary effect improves the density estimate in our case, as it allowed a sufficient number of patterns to contribute to the density estimate of points near the boundaries of the dataset. In contrast to the symmetric estimator, which underestimated densities near the boundary due to a lack of contributing points.

6 Conclusion

In conclusion we have that the shape adaptive Modified Breiman Estimator gives results comparable to those of the symmetric Modified Breiman Estimator. The estimator with kernels that are responsive to the data is better in estimating the density of points near the boundary of the dataset, especially if the dataset has multiple Gaussian components. Further research is required to determine if this boundary effect also occurs if the data points near th boundaries are not sampled from a uniform random distribution.

References

[1] Jon Louis Bentley. “Multidimensional Binary Search Trees Used for Associative Searching”. In: *Commun. ACM* 18.9 (1975), pp. 509–517. URL: `http://doi.acm.org/10.1145/361002.361007`.

[2] L. Breiman, W. Meisel, and E. Purcell. “Variable Kernel Estimates of Multivariate Densities”. In: *Technometrics* 19.2 (1977), pp. 135–144.

[3] V.A. Epanechnikov. “Non-Parametric Estimation of a Multivariate Probability Density”. In: *Theory of Probability & Its Applications* 14.1 (1969), pp. 153–158.

[4] B.J. Ferdosi et al. “Comparison of Density Estimation Methods for Astronomical Datasets”. In: *Astronomy & Astrophysics* 531 (2011).

[5] Wolfgang Härdle et al. *Nonparametric and semiparametric models*. Springer Series in Statistics. Springer Science & Business Media, 2012.

[6] Kirsty J Lees, Andrew J Guerin, and Elizabeth A Masden. “Using kernel density estimation to explore habitat use by seabirds at a marine renewable wave energy test facility”. In: *Marine Policy* 63 (2016), pp. 35–44.

[7] Johanna Skarpman Munter and Jens Sjőlund. “Dose-volume histogram prediction using density estimation”. In: *Physics in Medicine and Biology* 60.17 (2015), p. 6923.

[8] E. Parzen. “On Estimation of a Probability Density Function and Mode”. In: *The Annals of Mathematical Statistics* 33.3 (1962), pp. 1065–1076.

[9] B.W. Silverman. *Density Estimation for Statistics and Data Analysis*. Monographs on Statistics and Applied Probablity. Springer-Science+Business Media, B.V., 1986.

[10] M.H.F. Wilkinson and B.C. Meijer. “DATAPLOT: A Graphical Display Package for Bacterial Morphometry and Fluorimetry Data”. In: *Computer Methods and Programs in Biomedicine* 47.1 (1995), pp. 35–49.